TURBULENCE CHARACTERIZATION IN COMPRESSOR TANDEM BLADES AERODYNAMICS

***A. Rocca*[1], *M. Rasquin*[1], *Y. Marichal*[2], *K. Hillewaert*[3,1] *and T. Toulorge*[1]**

[1] ***Centre de Recherche en Aéronautique (Cenaero), Gosselies, Belgium***
[2] ***Safran Aero Boosters, Herstal, Belgium***
[3] ***Aerospace & Mechanics Department, Université de Liège (ULiège), Belgium***
michel.rasquin@cenaero.be

Abstract

Numerical simulations of a subsonic tandem compressor blade cascade ($Re_C = 3 \times 10^5$, $Ma_i = 0.6$) are carried out using wall-resolved implicit LES with a high-order discontinuous Galerkin method and RANS (SST and transitional $\mathrm{SST} - \gamma - Re_\theta$) with a finite-volume method. The wrLES serves as a high-fidelity reference for assessing RANS performance.

The isentropic Mach number on the blade surface and the total pressure losses in the wake are compared between wrLES and RANS. The transitional model captures qualitatively separation on the suction side of the front blade and the pressure side of the rear blade but fails to reproduce the unsteady wake–boundary-layer interaction on the suction side of the rear blade, predicting laminar separation and reattachment instead. In contrast, the standard SST model does not capture separation at all. In terms of losses, wrLES reveals an asymmetric two-humped profile with higher pressure-side losses in the wake, whereas RANS produces quasi-symmetric distributions.

Barycentric anisotropy analysis shows RANS solutions confined to the plane-strain line, while LES exposes richer turbulence states. Using SU2's EQUiPS, we quantify turbulence-model uncertainty on wake losses. The predicted band encloses most of the LES distribution, except at the pressure-side peak. This underscores the need for improved closures and the utility of uncertainty quantification for such applications.

1 Introduction

This study focuses on advancing turbulence modeling for turbomachinery applications. It presents the application of wall-resolved implicit Large-Eddy Simulation (wrLES) using the high-order Discontinuous Galerkin Method (DGM) to tandem compressor blades in a cascade configuration. The examined flow is subsonic, with no imposed inlet turbulence, and the operating condition corresponds to the design angle of attack. To the best of our knowledge, this research represents the first application of LES to this particular configuration. The primary objectives of this work are: (i) to generate accurate high-fidelity simulation data, and (ii) to provide insights into flow phenomena of particular relevance for designers. These objectives naturally motivate a detailed comparison with several Reynolds-Averaged Navier–Stokes (RANS) models, namely SST, SST–γ–Re_θ, and unsteady SST–γ–Re_θ, as RANS remains the industry standard for turbomachinery design. This study emphasizes advanced turbulence modeling aspects. These include assessing the validity of the Boussinesq hypothesis for the given setup, evaluating turbulence states in both RANS and LES, and analyzing their influence on flow predictions. Additionally, uncertainty quantification is conducted by introducing perturbations in the turbulence state, laying the groundwork for future development of machine-learning-based RANS closures. Renewed attention to tandem blades is triggered by sustainability targets in aviation, which demand radical innovations in engine design. Tandem blades achieve greater flow turning with lower global losses than single blades, making them strong candidates for replacing highly loaded axial compressor outlet guide vanes. However their aerodynamics challenges standard numerical methodologies. In tandem configurations, the wake of the front blade is not merely a loss source but plays an active role in performance. The interaction between the wakes and boundary layers, along with classical flow phenomena such as separation, reattachment, and laminar-turbulent transition, makes these cases highly relevant for study.

Traditional turbulence models struggle to accurately predict loss generation due to their inability to capture unsteady and anisotropic turbulence structures and mixing phenomena in the wake. High-fidelity numerical simulations, particularly LES, offer improved insights into turbulence evolution, vortex dynamics, and wake development. The objective of this study is to leverage advanced turbulence diagnostics to better understand flow physics and assess turbulence modeling approaches for turbomachinery applications. While their high computational cost discards any systematic use for design, scale-resolving simulations offer valuable insights and are increasingly exploited for RANS model calibration, training, validation and benchmarking (Akolekar, Waschkowski, Zhao, Pacciani, & Sandberg, 2021). Nevertheless, AI-enhanced Computational Fluid Dynamics remains in its infancy, requiring extensive training datasets

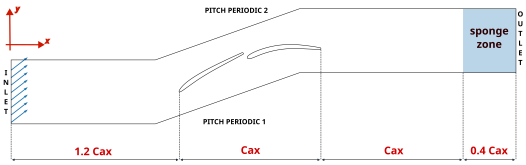

Figure 1: The computational domain

without guaranteed generalization. Meanwhile, industrial design still relies on turbulence models developed decades ago. Given these constraints, systematic validation of RANS models using uncertainty quantification (Gorlé, Zeoli, Emory, Larsson, & Iaccarino, 2019) and advanced visualization is crucial.

2 Application Case and Numerical Setup for wrLES

The tandem blade geometry used in this study was desgined at Cenaero. The cascade is modeled as a bi-periodic problem in pitch and span. The Reynolds number based on the total chord C is $Re_C = 300,000$, with an inlet Mach number $Ma_i = 0.6$. Air is modeled as a perfect gas. Boundary conditions include total quantities and flow direction at the inlet, static pressure at the outlet, and no-slip adiabatic conditions on the blades. The inflow is laminar.

The computational domain is shown in Figure 1. A sponge zone prevents acoustic wave reflections at the outlet and stabilizes the wake. The span length is 12% of the front blade's axial chord. A second-order unstructured hexa-dominant mesh, extruded in the spanwise direction using Gmsh, consists of 440, 000 cells and is shown in Figure 2. The discontinuous Galerkin spatial discetization is based on third-order P3 element-wise polynomials, yielding a fourth-order accurate scheme with a total 30×10^6 degrees of freedom per equation (dof/eq).

On both the front and rear blades, the grid resolution complies with the standard wrLES guidelines, namely, with $n^+ < 1$, $s^+ < 25$ and $z^+ < 25$, where n^+, s^+ and z^+ denote the local wall-normal, (streamwise) wall-tangential and spanwise coordinates respectively, expressed in wall-units.

Time integration is performed using a second-order implicit backward differentiation formula. Further details on the numerical method implemented in the Argo solver can be found in Carton de Wiart, Hillewaert, Bricteux, and Winckelmans (2015).

3 RANS Simulations

In parallel to the wall resolved LES, a RANS campaign was carried out with the open-source code SU2 (v8.1.0) (Economon, Palacios, Copeland, Lukaczyk, & Alonso, 2016), using two turbulence closures: the SST k–ω model (2003m modification described in Menter, Kuntz, and Langtry (2003)) and the transitional SST $-\ \gamma\ -\ Re_\theta$ model (Menter, Langtry, &

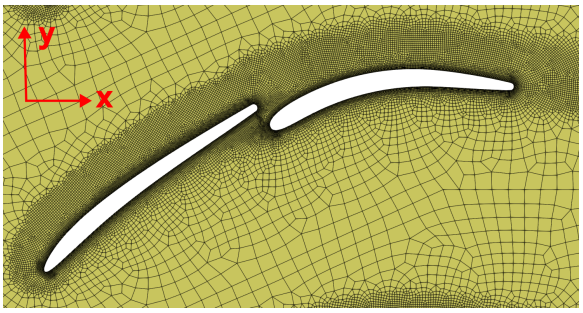

Figure 2: Computational grid for WRLES simulations

Völker, 2006; Langtry & Menter, 2009). The setup matches the wrLES fluid properties and boundary conditions, but in a purely 2D domain discretized with roughly 50,000 quadrangles. The mesh ensures $n^+ < 1$ near walls, with a refinement study performed prior to the final choice. Inlet turbulence conditions were set to $I = 0.5\%$ and $\mu/\mu_t = 10$. Numerical schemes include Green–Gauss gradients, Roe flux with MUSCL (2nd order upwind) for convection, 1st-order upwind for turbulence terms, and the restarted FGMRES for the linear solver.

4 Results and analysis

Wake - Boundary layer interaction

Figure 3 presents a numerical Schlieren visualization obtained with Argo, where the instantaneous quantity $|\nabla\rho|/\rho$ is used to provide a qualitative representation of the flow dynamics. The visualization was produced using a dedicated ParaView plugin specifically designed to process high-order polynomial solutions (Rasquin, Bauer, & Hillewaert, 2019).

Laminar separation bubbles originate at the leading edge of the front blade, triggering separation-induced transition on both its pressure and suction sides (marked as 1 and 2 in Figure 3), as well as on the pressure side of the rear blade (3). In the tandem configuration, the wake shed by the front blade (4) plays a decisive role: it constrains the flow accelerating through the inter-blade passage, thereby suppressing separation on the suction side of the rear blade and allowing it to sustain a higher aerodynamic load. In the present setup, where the blade gap is relatively short, this wake directly interacts with the boundary layer on the rear blade suction side (4), dictating the transition process and promoting a bypass-type mechanism (Ovchinnikov, Choudhari, & Piomelli, 2008). Further downstream, the wakes (3, 6) spread and merge (5), while the bifurcation of the front-blade wake is highlighted in (7).

Turbulent BL and wake analysis

Figure 4 compares the isentropic Mach number obtained from wrLES with the RANS predictions. The

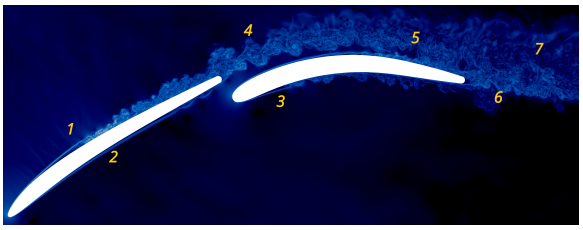

Figure 3: Turbulent flow visualization using $\nabla\rho/\rho$

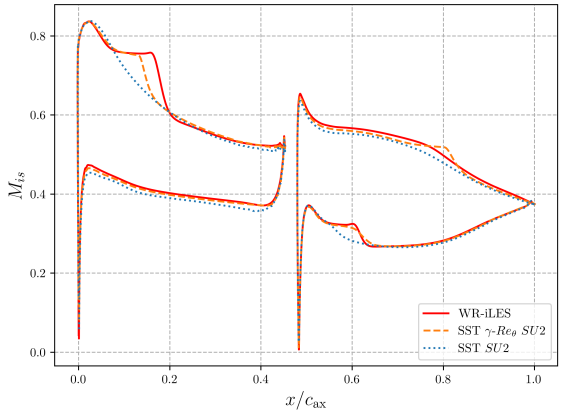

Figure 4: Isentropic Mach number on the blade surface

isentropic Mach number, M_{is}, is defined as

$$M_{is} = \sqrt{\left[\left(\frac{p_t^i}{p}\right)^{\frac{\gamma-1}{\gamma}} - 1\right]\frac{2}{\gamma-1}},, \qquad (1)$$

where p_t^i denotes the inlet total pressure and $\gamma = 1.4$. At $x/\mathrm{C_{ax}} = 0$, all three curves collapse, indicating consistent inlet conditions across the simulations. On the suction side of the front blade, the transitional SST–γ–Re_θ model qualitatively captures flow separation, unlike the standard SST model, which proves inadequate for the present configuration. A similar behavior is observed on the pressure side of the rear blade. However, on its suction side, the semi-empirical formulation of the SST–γ–Re_θ model fails to reproduce the unsteady wake–boundary-layer interaction. Instead, it predicts laminar separation followed by reattachment and transition, analogous to the behavior observed on the front blade.

These modeling uncertainties strongly affect the downstream flow evolution, underlining the limitations of RANS closures in such conditions. Notably, the RANS models predict an exit flow angle of nearly $1.5°$ upward, whereas wrLES yields a slightly negative value.

Figure 5 presents the loss coefficient ω along the non-dimensional pitch coordinate η, defined as

$$\omega = \frac{p_t^i - \overline{p_t(\eta)}}{p_t^i - \overline{p_s^i}}, \qquad \eta = \frac{y - \min(y)}{\text{pitch}}, \qquad (2)$$

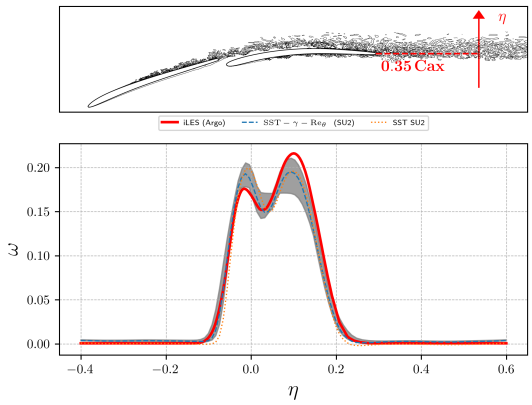

Figure 5: Total pressure losses in the wake for wrLES, RANS (SST and SST–γ–Re_θ), and the corresponding uncertainty quantification from EQUiPS

where p_t^i is the prescribed inlet total pressure, $\overline{p_s^i}$ the time- and span-averaged inlet static pressure, and $\overline{p_t(\eta)}$ the time- and span-averaged total pressure measured at $x = 0.35, \mathrm{C_{ax}}$ downstream of the rear blade trailing edge.

In tandem configurations, the total-pressure-loss distribution exhibits a characteristic two-humped profile, associated with each blade wake. The wrLES in red predicts an asymmetric distribution, with larger losses originating from the pressure sides of the blades. By contrast, both RANS models yield lower pressure-side losses and higher suction-side losses, resulting in a quasi-symmetric profile of ω. These discrepancies can be attributed to differences in the modeled mechanisms of turbulent kinetic energy production and dissipation. More details of this analysis can be found in Rocca, Rasquin, Hillewaert, Al Rifai, and Toulorge (2025).

Boussinesq approximation

The limitations of RANS turbulence modeling are well-known, particularly in the context of accurately capturing such intricate flows. To enhance our understanding not only of the underlying physics but also of the predictive tools used in engineering design, it is interesting to examine the validity of the Boussinesq Hypothesis (BH) of linear eddy viscosity, which assumes linearity between the Reynolds stress tensor (RST) $\rho\overline{u_i'u_j'}$ and the mean strain rate tensor $\overline{S}_{ij}$. The Boussinesq Hypothesis (BH), which forms the basis of most RANS turbulence models, expresses the RST as

$$-\rho\,\overline{u'_i u'_j} = 2\,\mu_t\left(\overline{S}_{ij} - \frac{1}{3}\frac{\partial U_k}{\partial x_k}\delta_{ij}\right) - \frac{2}{3}k\rho\delta_{ij}, \qquad (3)$$

where the mean strain rate tensor is defined as

$$\overline{S}_{ij} = \frac{1}{2}\left(\frac{\partial U_i}{\partial x_j} + \frac{\partial U_j}{\partial x_i}\right), \qquad (4)$$

and where $k = \frac{1}{2}\overline{u'_i u'_i}$ is the turbulent kinetic energy.

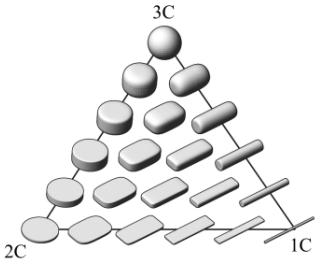

Figure 6: Representative tensor shapes in the barycentric triangle from Jofre, Domino, and Iaccarino (2018)

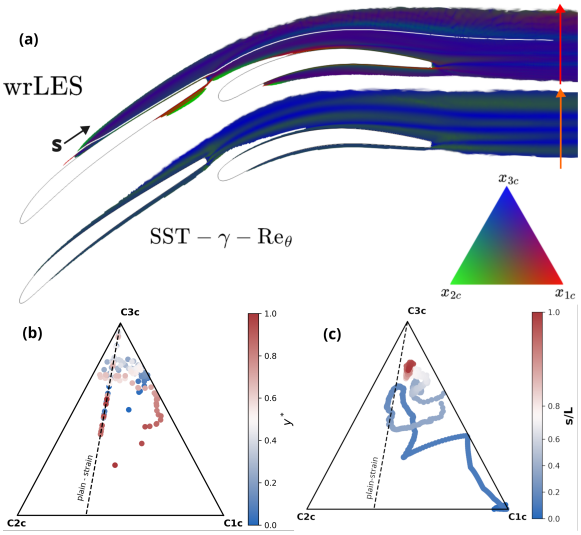

Figure 7: Barycentric analysis of the turbulence state in the wake and along a streamline

Barycentric map

Banerjee, Krahl, Durst, and Zenger (2007) introduced a barycentric representation of turbulence anisotropy based on the normalized Reynolds stress anisotropy tensor, defined as

$$a_{ij} = \frac{\overline{R}^a_{ij}}{2k}, \tag{5}$$

with

$$\overline{R}^a_{ij} = \rho\overline{u'_i u'_j} - \tfrac{2}{3}\rho k\delta_{ij}. \tag{6}$$

This formulation provides a linear mapping of anisotropy states, ensuring that the three limiting states of turbulence (one-component, two-component, and isotropic) are weighted equally within the barycentric triangle. Building on this framework, Emory and Iaccarino (2014) proposed a direct mapping to an RGB color scheme to facilitate visualization: one-component turbulence is assigned red (bottom-right corner), two-component turbulence green (bottom-left corner), and isotropic turbulence blue (top corner), with intermediate anisotropy states appearing as color blends across the interior of the triangle.

A sketch of the tensor shapes extracted from Jofre, Domino, and Iaccarino (2018) is presented in Figure 6.

Figure 7(a) depicts the turbulence state for the tandem blade configuration, comparing wrLES (top) with the transitional $\mathrm{SST}-\gamma-Re_\theta$ model (bottom). Figure 7(b) shows the evolution of the turbulence state in the wake for both approaches. The extraction line through the wake is indicated in Figure 7(a) by a red vertical arrow for wrLES and an orange vertical arrow for $\mathrm{SST}-\gamma-Re_\theta$. The colormap corresponds to the normalized pitch coordinate, η. It is worth noting that all RANS data collapse onto the plane-strain turbulence line, shown as a dashed line in Figure 7(b), which by construction connects the isotropic corner (top) to a point on the lower edge of the barycentric triangle located one third of the edge length from the two-component corner. In the wake, the $\mathrm{SST}-\gamma-Re_\theta$ model generally predicts turbulence as either isotropic or plane-strain (along the dashed line). In contrast, wrLES demonstrates that, within the wake, the turbulence more closely approaches an axisymmetric expansion limit state (1C $\Rightarrow$ 3C). The RST evolves such that the stress ellipsoid transitions from a thin, elongated rod shape, gradually thickens, and may eventually become spherical in the case of isotropic turbulence, as depicted in Figure 6.

Figure 7(c) presents a similar analysis along a streamline highlighted in Figure 7(a), shown for the wrLES only. The streamline originates near the leading edge, with s/L denoting the non-dimensional distance from its origin. The colormap is customized such that the white marker corresponds to the trailing edge of the rear blade.

Along this streamline, turbulence initially exhibits a one-component (simple-shear) state near the blade surface, where the boundary layer remains laminar. Following the laminar separation bubble and transition, the RST rapidly deforms and aligns with the strain rate along the plane-strain line. As the flow separates at the trailing edge of the front blade and convects into the wake, the RST departs from plane-strain characteristics and evolves between the 1C and 3C regions. Downstream of the rear-blade trailing edge, no further significant changes occur, and the red markers cluster tightly in the isotropic region of the triangle.

Uncertainty quantification

The modeled Reynolds stress tensor is often unable to reproduce the correct physics of complex flows, which directly affects the prediction of turbulent kinetic energy (TKE) production. To quantify this model-form uncertainty, we employ the EQUiPS module (Enabling Quantification of Uncertainty in Physics-based Simulations) implemented in SU2 (Iaccarino, Mishra, & Ghili, 2017; Thompson, Mishra, Iaccarino, Edeling, & Sampaio, 2019). The methodology perturbs the Reynolds stress tensor in its eigenspace, expressed in terms of its eigenvalues and

eigenvectors:

$$R_{ij}^{\star} = 2\rho k^{\star} \left(\frac{\delta_{ij}}{3} + v_{in}^{\star} \, \Lambda_{nl}^{\star} \, v_{lj}^{\star} \right), \qquad (7)$$

where the superscript $\star$ denotes perturbed quantities.

Eigenvalue perturbations modify the *shape of the Reynolds stress ellipsoid* (Pope, 2000; Jofre *et al.*, 2018), corresponding to changes in the turbulence componentality. In the barycentric map, such perturbations are characterized by both a *direction* (towards a limiting state) and a *magnitude* (the distance traveled along that direction). Specifically, perturbations are directed toward the three vertices of the barycentric triangle: $\mathbf{x}_{1C}$, $\mathbf{x}_{2C}$, and $\mathbf{x}_{3C}$, representing the one-component, two-component, and isotropic limiting states of anisotropy, respectively. The perturbation magnitude is controlled by the parameter $\Delta_B \in [0, 1]$: $\Delta_B = 0$ corresponds to the baseline model prediction, while $\Delta_B = 1$ projects the state fully onto the target vertex.

The perturbed barycentric coordinates are given by

$$\mathbf{x}^{\star} = \mathbf{x} + \Delta_B \left(\mathbf{x}^{\mathbf{t}} - \mathbf{x} \right), \qquad (8)$$

where $\mathbf{x}^{\mathbf{t}}$ is the target vertex and $\mathbf{x}$ is the baseline model prediction.

In the present work, we adopt the default EQUiPS settings with $\Delta_B = 1.0$, so that all three limiting states are explicitly considered. This provides an envelope of possible turbulence anisotropy realizations against which the sensitivity of the modeled TKE production can be assessed.

Figure 5 illustrates the uncertainty band for the loss coefficient ω, shown in gray, obtained by perturbing the modeled Reynolds stress tensor of the $\mathrm{SST} - \gamma - Re_\theta$ model. These perturbations modify the production term of turbulent kinetic energy and thereby alter the associated dissipation mechanisms.

The loss coefficient predicted by wrLES lies almost entirely within the uncertainty band of the $\mathrm{SST} - \gamma - Re_\theta$ model, with the exception of the loss peak on the blade pressure side, which falls slightly outside the envelope. One reason for this is that the perturbations are applied sequentially in independent RANS simulations and each realization imposes a spatially uniform modification of the turbulence state across the entire domain. Nevertheless, considering only $\mathbf{x}^t \in [\mathbf{x}_{1C}, \mathbf{x}_{2C}, \mathbf{x}_{3C}]$ with $\Delta_B = 1.0$ already provides a reasonable estimate of the uncertainty band for the pressure loss predicted by the $\mathrm{SST} - \gamma - Re_\theta$ model.

5 Conclusions and perspectives

This study examined a tandem compressor blade cascade using wall-resolved LES and RANS simulations, with LES serving as a high-fidelity reference for assessing RANS model performance. The results confirm the influence of the front-blade wake on cascade dynamics, particularly through its unsteady interaction with the rear-blade boundary layer. These effects underline the importance of scale-resolving simulations for understanding tandem designs.

Front-blade transition remains a key uncertainty, and its accurate prediction requires careful application of transition models. The comparisons show that while the transitional SST–γ–Re_θ model captures certain separation–transition mechanisms, it fails to reproduce wake–boundary-layer interactions, resulting in discrepancies in Mach number distributions, loss predictions, and exit flow angles. The barycentric analysis demonstrates that RANS solutions collapse onto the plane-strain line, whereas LES reveals richer turbulence anisotropy states, highlighting the limitations of the linear eddy-viscosity assumption.

Uncertainty quantification with the SU2 EQUiPS module provides valuable envelopes for the loss coefficient by perturbing the Reynolds stress tensor in its eigenspace. The LES results lie almost entirely within these uncertainty bands, with deviations confined mainly to pressure-side losses. Although the present perturbations impose spatially uniform modifications, the approach remains a practical means of quantifying RANS model-form uncertainty in turbomachinery flows.

Beyond the present results, this work provides a high-fidelity dataset for the development of improved turbulence closures, including machine-learning-based approaches. Future extensions of this research will address off-design operating conditions, inlet turbulence injection and RANS model calibration and correction with uncertainty quantification. Ultimately, these efforts aim to advance turbulence modeling capabilities and provide more reliable tools for sustainable turbomachinery design.

Acknowledgments

The authors would like to thank Safran Aero Boosters for their permission to publish this work. The presented work has been performed in the framework of the WINGS project, funded by the Walloon Region in Begium under grant agreement n°8441. The present research benefited from computational resources made available on the Tier-1 supercomputer of the Fédération Wallonie-Bruxelles, infrastructure funded by the Walloon Region under the grant agreement n°1117545. We acknowledge EuroCC Belgium for awarding this project access to the LUMI supercomputer hosted by CSC (Finland) and the LUMI consortium, through the allocation Cenaero-HiFiDBTurb-T0331.

References

Akolekar, H. D., Waschkowski, F., Zhao, Y., Pacciani, R., & Sandberg, R. D. (2021). Transition modeling for low pressure turbines using computational fluid dynamics driven machine learning. Energies, 14(15). doi: 10.3390/en14154680

Banerjee, S., Krahl, R., Durst, F., & Zenger, C. (2007). Presentation of anisotropy properties of turbulence, invariants versus eigenvalue approaches. Journal of Turbulence(8).

Carton de Wiart, C., Hillewaert, K., Bricteux, L., & Winckelmans, G. (2015). Implicit LES of free and wall-bounded turbulent flows based on the discontinuous Galerkin/symmetric interior penalty method. International Journal for Numerical Methods in Fluids, 78. doi: 10.1002/fld.4021

Economon, T. D., Palacios, F., Copeland, S. R., Lukaczyk, T. W., & Alonso, J. J. (2016). SU2: An open-source suite for multiphysics simulation and design. AIAA Journal, 54(3), 828–846.

Emory, M., & Iaccarino, G. (2014). Visualizing turbulence anisotropy in the spatial domain with componentality contours. In Center for turbulence research. annual research briefs 2014.

Gorlé, C., Zeoli, S., Emory, M., Larsson, J., & Iaccarino, G. (2019, 03). Epistemic uncertainty quantification for Reynolds-averaged Navier-Stokes modeling of separated flows over streamlined surfaces. Physics of Fluids, 31(3), 035101. doi: 10.1063/1.5086341

Iaccarino, G., Mishra, A., & Ghili, S. (2017). Eigenspace perturbations for uncertainty estimation of single-point turbulence closures. Physical Review Fluids, 2. doi: 10.1103/PhysRevFluids.2.024605

Jofre, L., Domino, S. P., & Iaccarino, G. (2018). A Framework for Characterizing Structural Uncertainty in Large-Eddy Simulation Closures. Flow, Turbulence and Combustion, 100, 341-363.

Langtry, R. B., & Menter, F. R. (2009). Correlation-Based Transition Modeling for Unstructured Parallelized Computational Fluid Dynamics Codes. AIAA Journal, 47(12), 2894-2906. doi: 10.2514/1.42362

Menter, F., Kuntz, M., & Langtry, R. (2003, 01). Ten years of industrial experience with the SST turbulence model. Heat and Mass Transfer, 4.

Menter, F., Langtry, R. B., & Völker, S. (2006, 10). Transition Modelling for General Purpose CFD Codes. Flow, Turbulence and Combustion, 77, 277-303. doi: 10.1007/s10494-006-9047-1

Ovchinnikov, V., Choudhari, M. M., & Piomelli, U. (2008). Numerical simulations of boundary-layer bypass transition due to high-amplitude free-stream turbulence. Journal of Fluid Mechanics, 613, 135–169.

Pope, S. B. (2000). Turbulent Flows. Cambridge University Press.

Rasquin, M., Bauer, A., & Hillewaert, K. (2019). Scientific post hoc and in situ visualisation of high-order polynomial solutions from massively parallel simulations. International Journal of Computational Fluid Dynamics.

Rocca, A., Rasquin, M., Hillewaert, K., Al Rifai, A., & Toulorge, T. (2025). Wall-Resolved iLES of Compressor Tandem-Blades Using High-Order DG Method. In Turbo expo (Vol. 88872, p. V011T32A006).

Thompson, R., Mishra, A., Iaccarino, G., Edeling, W., & Sampaio, L. (2019). Eigenvector perturbation methodology for uncertainty quantification of turbulence models. Physical Review Fluids, 4. doi: 10.1103/PhysRevFluids.4.044603